



Network analysis of 16S rRNA sequences suggests microbial keystone taxa contribute to marine N₂O cycling

Brett D. Jameson¹, Sheryl A. Murdock^{2,3}, Qixing Ji^{3,4}, Catherine J. Stevens¹, Damian S. Grundle^{3,5} & S. Kim Juniper^{1,2,6}

The mechanisms by which large-scale microbial community function emerges from complex ecological interactions between individual taxa and functional groups remain obscure. We leveraged network analyses of 16S rRNA amplicon sequences obtained over a seven-month timeseries in seasonally anoxic Saanich Inlet (Vancouver Island, Canada) to investigate relationships between microbial community structure and water column N₂O cycling. Taxa separately broadly into three discrete subnetworks with contrasting environmental distributions. Oxycline subnetworks were structured around keystone aerobic heterotrophs that correlated with nitrification rates and N₂O supersaturations, linking N₂O production and accumulation to taxa involved in organic matter remineralization. Keystone taxa implicated in anaerobic carbon, nitrogen, and sulfur cycling in anoxic environments clustered together in a low-oxygen subnetwork that correlated positively with nitrification N₂O yields and N₂O production from denitrification. Close coupling between N₂O producers and consumers in the anoxic basin is indicated by strong correlations between the low-oxygen subnetwork, PICRUSt2-predicted nitrous oxide reductase (*nosZ*) gene abundances, and N₂O undersaturation. This study implicates keystone taxa affiliated with common ODZ groups as a potential control on water column N₂O cycling and provides a theoretical basis for further investigations into marine microbial interaction networks.

¹School of Earth & Ocean Sciences, University of Victoria, P.O. Box 1700 Station CSC, Victoria, BC V8W 2Y2, Canada. ²Department of Biology, University of Victoria, P.O. Box 1700 CSC, Victoria, BC V8W 2Y2, Canada. ³Bermuda Institute of Ocean Sciences, 17 Biological Station, St. George's GE01, Bermuda. ⁴Thrust of Earth, Ocean & Atmospheric Sciences, Hong Kong University of Science and Technology (Guangzhou), Nansha, Guangzhou, Guangdong 511400, China. ⁵School of Ocean Futures & School of Earth & Space Exploration, Arizona State University, Tempe, AZ 85287-7904, USA. ⁶Ocean Networks Canada, 2474 Arbutus Road, Victoria, BC V8N 1V8, Canada. ✉email: bjameson@uvic.ca

Linking the dynamics of complex marine microbial communities to ecosystem-scale biogeochemical processes is one of the foremost challenges in the field of microbial ecology^{1,2}. The application of high-throughput gene sequencing and meta-omics to surveys of marine microbial communities has resulted in a growing awareness of the ubiquity, throughout the microbial phylogenetic tree and across a broad range of environments, of enzyme-encoding functional genes responsible for mediating core biogeochemical cycles^{3,4}. Functional genes of this sort co-vary strongly with environmental variables, leading to an emerging view of microbial communities as meta-organisms rather than assemblages of interacting taxa^{5,6}. From a biogeochemical point of view, proximal, abiotic controls on rate processes can now be seen as shaping genomes, transcriptomes and proteomes across environmental gradients, rather than simply modulating inputs and outputs from microbial black boxes^{7–9}. This is especially true for marine oxygen deficient zones (ODZs) and sulfidic basins, where sharp redox gradients constrain the taxonomic identity and metabolic potential of microbial constituents, as well as the character of key biogeochemical transformations^{7,10,11}. Robust patterns of metabolic niche differentiation have since led to the development of conceptual models that describe coupled metabolic interactions between key players across vertical redox gradients^{7,12}. However, from an ecological point of view, the meta-organism paradigm provides limited insight into the mechanisms that drive community assembly at the taxonomic level, and how ecosystem function arises from a complex network of biogeochemical and ecological interactions between individual taxa.

Ecosystem function is an emergent phenomenon that results from the cumulative set of metabolic and ecological interactions that characterize dynamic and co-evolving microbial communities in the environment¹³. These interactions occur at the microscopic level and involve numerous individual taxa with diverse functional capacities. Individual cells, strains, or functional groups within a community can influence each other through a multitude of mechanisms, including mutualistic cross-feeding¹⁴, resource competition¹⁵, the production of public goods¹⁶ or allelopathic compounds¹⁷, and many others¹⁸. Unfortunately, ecological interactions of this sort are difficult to characterize given the cryptic nature of natural microbial communities. Complicating matters further is the fact that the vast majority of microbial organisms remain uncultured, and thus taxonomically and functionally ambiguous. Fortunately, improvements to high-throughput sequencing technologies and data processing tools combined with novel statistical approaches have allowed researchers to study patterns of microbial community assembly in unprecedented detail^{19–21}.

Network analyses applied to the study of complex microbial communities has resulted in a corpus of literature documenting spatiotemporal co-occurrence patterns amongst microbial community members across a wide range of terrestrial and aquatic ecosystems^{22–24}. These tools go beyond traditional assessments of biodiversity and community structure by utilizing pairwise correlations between individual taxonomic units to identify core community members and assess co-occurrences between individual taxa. Although the mechanisms driving specific co-occurrences cannot be discerned from network analyses alone, parallel information on rate processes and environmental variables can help generate testable hypotheses regarding putative ecological interactions responsible for driving ecosystem function¹¹. This is a potentially fruitful line of investigation, given recent progress in linking microbial community structure to large-scale ecosystem processes such as carbon export, nitrogen fixation, and denitrification^{25–27}. A holistic approach to the study of marine biogeochemical processes that encapsulates the internal

complexity of entire communities may also help to elucidate ecological controls that have been previously overlooked by a reductionist focus on protein-encoding functional genes.

Empirical and computational studies suggest that microbial communities contain keystone members, defined as highly connected taxa that exert considerable influence over community structure and function irrespective of their abundances across space and time²⁸. Keystone taxa can exist independently or may also be part of keystone guilds comprising several taxa of similar niche-preferences and functional properties²⁶. More importantly, keystone taxa may exert influence over ecosystem processes directly, such as through the production or utilization of shared metabolites²⁹, or indirectly by modulating the broader community structure³⁰. This evidence suggests that ecological interactions between functionally diverse microorganisms may underlie more subtle relationships between microbial community structure and ecosystem function.

The microbial production and consumption of nitrous oxide (N₂O) is a timely area of focus for investigating links between microbial community dynamics and ecosystem processes. Nitrous oxide is currently the third most important greenhouse gas behind CO₂ and methane and is the predominant ozone-depleting substance emitted in the 21st century^{31,32}. Current models estimate that marine ecosystems account for 10 to 53% of the annual global N₂O emissions, leaving much to be learned about the drivers of spatiotemporal variability³³. In the marine environment, N₂O is produced primarily as a by-product of ammonium oxidation or as a free-intermediate in the sequential reduction of nitrate and nitrite to dinitrogen gas (N₂) during heterotrophic or sulfide-driven denitrification³⁴. Elevated rates of production from both pathways are observed near the boundaries of marine oxygen deficient zones (ODZs) and anoxic basins where oxidative and reductive processes are closely coupled in space and time^{35–37}. Conversely, the reduction of N₂O to N₂ by organisms possessing N₂O-reductases is the only confirmed biological sink for N₂O and can drive N₂O concentrations toward undetectable levels in some anoxic water masses^{38,39}. Nitrous oxide cycling is thus the product of distributed metabolic networks that involve syntrophic interactions between important players in the biogeochemical cycling of carbon, nitrogen, and sulfur, with net fluxes likely determined by a complex interplay between environmental and biological factors.

Saanich Inlet is a well-studied, seasonally euxinic fjord located on Vancouver Island, Canada that is characterized by extreme seasonal shifts in water column redox gradients driven by cycles of primary production and physical mixing^{40–42}. The inlet is further distinguishable from open ocean ODZs by its restricted depths (~225 m maximum) and the presence of sulfidic bottom water throughout much of the year^{43–45}. However, the reliable transition between periods of water column stagnation and bottom water anoxia, and oxygenation of the deep basin following deep water renewal provides a unique opportunity to explore links between biogeochemical rate processes and microbial community dynamics under changing redox conditions^{46,47}. Furthermore, studies focusing on microbial community dynamics in easily accessible anoxic basins with reliable sulfide accumulation are useful for understanding trajectories in coastal systems experiencing increases in the frequency of bottom water hypoxia and transient sulfidic conditions^{48–50}. Previous work in Saanich Inlet suggests that N₂O production is driven by ammonium oxidation at oxycline depths, with substantial contributions from reductive processes near the base of the oxycline during periods of bottom-water anoxia and in the deep basin following renewal events^{44,51}. However, little is currently known about the role of keystone taxa, and ecological interactions more broadly, in mediating N₂O-cycling rate processes across marine redox gradients.

This study combines high-throughput sequencing of microbial 16S rRNA amplicons, in situ rate measurements, and environmental characterizations collected in Saanich Inlet over a bi-monthly timeseries between April and October 2018. We leverage network and multivariate statistical analyses to separate co-occurring taxa into discrete subnetworks with contrasting ecological distributions and roles in water column N₂O cycling. Oxycline subnetworks were correlated with nitrification rates and N₂O supersaturations and contained keystone taxa implicated in aerobic organic matter remineralization, including members of the ubiquitous SAR11 group. Members of the low-oxygen subnetwork demonstrated a preference for anoxic and N₂O-undersaturated waters and contained keystone taxa belonging to groups associated anaerobic carbon, nitrogen, and sulfur cycling such as SUP05. Taxa identified as potential keystones belonged to groups found throughout global ODZs and anoxic basins, thus providing a theoretical basis for further investigations into the importance of ecological interactions in regulating marine N₂O production and accumulation.

Results

Microbial community structure. We generated 818,133 paired-end microbial 16S rRNA gene sequence reads across 24 samples. A total of 469,628 bacterial and 211,767 archaeal reads remained following sequence merging and quality filtering, resulting in 168 archaeal and 2814 bacterial non-singleton amplicon sequence variants (ASVs). Mean amplicon lengths were 437 and 445 bp for bacterial and archaeal sequences, respectively. The total number of merged reads for each sample following quality control are reported in Supplementary Table 2.

The Saanich Inlet microbial community was well-stratified in April and demonstrated stark shifts in bacterial community structure across depth-dependent redox gradients (Fig. 1a). Members of the SAR11 α -proteobacteria dominated bacterial sequence reads between 75 and 100 m (~35%), along with high abundances of Rhodobacterales (9–27%) and Flavobacteriales (4–9%). These groups decreased in prominence with depth along the oxycline, collectively accounting for <1% of sequence reads below the anoxic interface (130 and 160 m). ASVs belonging to the SUP05 γ -proteobacteria showed contrasting distributions, with maximum values observed in the lower oxycline and anoxic basin between 110 and 160 m (39–41%). Other prominent taxa of the low-oxygen communities included members of the Marinimicrobia (2–4%), Ectothiorhodospirales (6–11%), and Desulfobacterales (0.3–6%). Members of the *Nitrospina* genus within the order Nitrospinales also reached peak relative abundances of 1–1.5% in the lower oxycline and anoxic basin samples despite pronounced vertical stratification of individual ASVs.

Archaeal sequence reads were dominated by Thaumarchaeota ASVs that mapped to two genera within the *Nitrosopumilaceae* family (Fig. 1b). A single *Nitrosopumilus*-like ASV (ARCH1) accounted for 56–86% of all archaeal sequences and was uniformly distributed across water column depths and sampling dates (Supplementary Fig. 2b). Lower oxycline and anoxic basin samples were characterized by increases in the abundance of a second, low-oxygen *Nitrosopumilus* ecotype (ARCH3) with maximum values of over 25% of *Nitrosopumilaceae* reads between 110 and 160 m alongside ASVs belonging to the *Bathyarchaeia* and Thermoplasmata. In contrast, thaumarchaeotal communities of the upper oxycline contained higher abundances of *Nitrosopelagicus*-like variants (Fig. 1, Supplementary Fig. 2b). Members of the Marine Group II (MGII) and Marine Group III (MGIII) Euryarchaeota also reached peak relative abundances in upper oxycline samples (~33% and 2%, respectively), and decreased precipitously with depth (Fig. 1b).

At least three discrete renewal events were detected at variable depths prior to sampling in June, August, and October, resulting in substantial changes to water column redox gradients and microbial community structures across renewal depths⁵¹. Renewal events prior to June and August sampling impacted midwater depths between 75 and 150 m, while October renewal was associated with oxygenation of the deep basin below 160 m. Increases in dissolved O₂, NO₃⁻, and N₂O concentrations across renewal depths were associated with elevated abundances of SAR11, *Rhodobacteraceae* and *Flavobacteraceae* ASVs in addition to vertical homogenization of the Archaeal community (Fig. 1). These events were generally accompanied by decreases in the relative abundance of SUP05, Marinimicrobia, Ectothiorhodospirales, and Desulfobacterales ASVs at deeper renewal depths and upward transport to 75 and 90 m ostensibly resulting from uplift of anoxic basin waters and subsequent mixing with renewal waters. Progressive increases in the prevalence of ASVs belonging to the Campylobacterales were also detected at 130 and 160 m between April and August. Campylobacterales reads were dominated by a single *Arcobacter* ASV that accounted for between 25% and 57% of total bacterial reads at 160 m in June and August, respectively. Conversely, *Nitrospina* ASVs increased in relative abundance with time throughout much of the water column, with peak values of approximately 3% occurring at mid-depth in October despite variable depth-related trends between sampling dates.

Clustering of bacterial and archaeal communities via non-metric multidimensional scaling (NMDS) followed water column N₂O saturations (Δ N₂O), with samples from undersaturated waters grouping together closely (Fig. 2). Envfit analysis implicated NO₃⁻ concentrations as the strongest predictor of community structure for both bacterial ($r^2 = 0.82$, $p = 0.001$) and archaeal ($r^2 = 0.77$, $p = 0.001$) ASVs. Secondary predictors for both domains included dissolved O₂ concentrations, NH₄⁺ concentrations and Δ N₂O. The influence of dissolved O₂ on NMDS ordinations was stronger for bacterial communities ($r^2 = 0.70$, $p = 0.001$) than for archaeal communities ($r^2 = 0.65$, $p = 0.001$), while Δ N₂O showed greater influence over archaeal community structure ($r^2 = 0.65$, $p = 0.001$ for Archaea versus $r^2 = 0.57$, $p = 0.001$ for Bacteria). In contrast, the influence of NH₄⁺ concentration was similar between the bacterial ($r^2 = 0.69$, $p = 0.001$) and archaeal domains ($r^2 = 0.71$, $p = 0.002$). Temperature and salinity were also implicated as potential drivers of community structure, although correlational strengths were lower in comparison to other variables ($r^2 = 0.47$ – 0.52 , $p = 0.001$ – 0.015).

N₂O-cycling community networks. We performed two separate network-level analyses on the combined, centred-log ratio (clr) transformed bacterial and archaeal ASV tables to explore patterns of community assembly and relationships between community interaction networks and N₂O cycling. A total of 38 archaeal and 324 bacterial ASVs were included in the network-level analyses following removal of low abundance taxa to improve interpretability and minimize the risk of spurious correlations. First, we used proportionality analyses to define a community co-occurrence network of interacting taxa with absolute rho values >0.60 (Fig. 3). These results were then compared with those obtained through weighted gene correlational network analysis (WGCNA) of the same dataset to identify core community members and elucidate links between microbial community structure and N₂O production processes. Relationships between entire community subnetworks and N₂O production were assessed by correlating subnetwork eigengenes with relevant sample traits (environmental variables and measured rates). The potential role of community structure in mediating water column

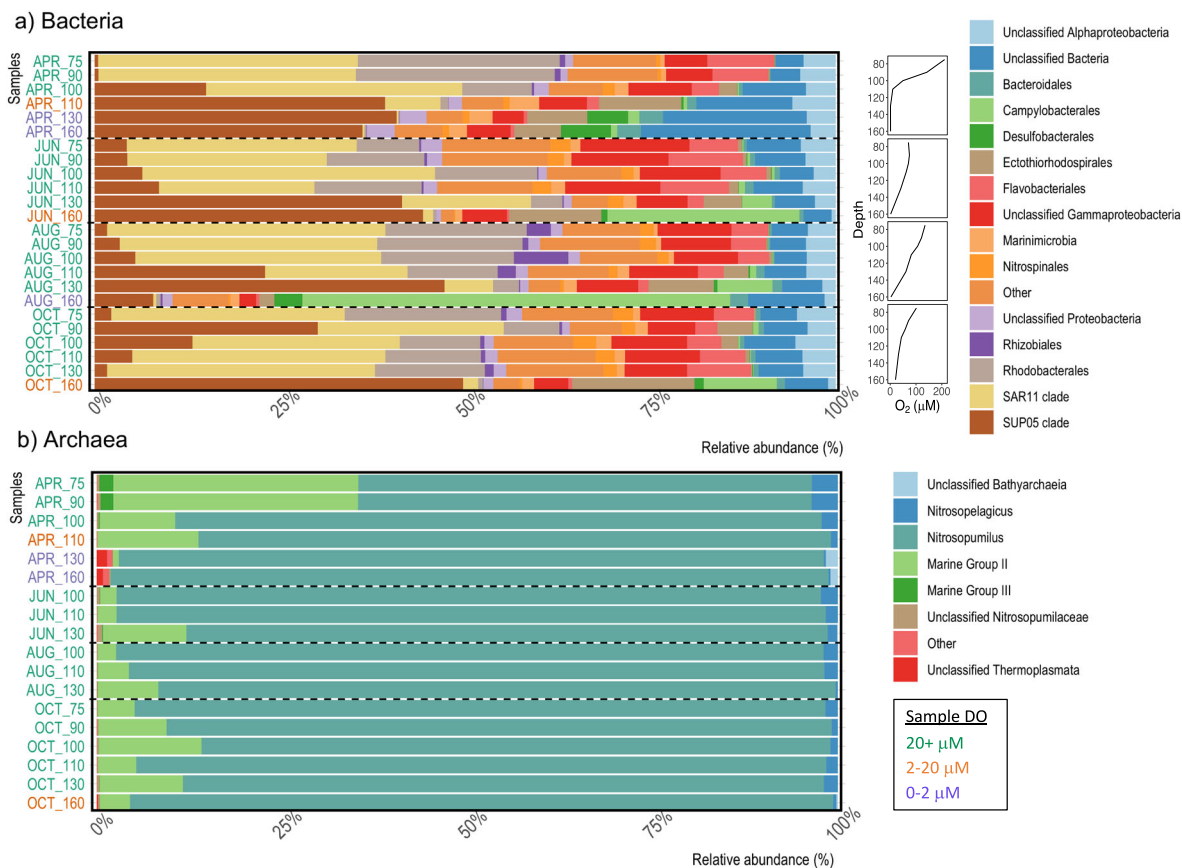


Fig. 1 Bacterial and archaeal community structure. Compositional barplots showing relative abundances of **a** Bacteria and **b** Archaea ASVs in Saanich inlet seston samples. Dissolved oxygen profiles for each sampling period are reported in panel **(a)**. Samples were obtained from Saanich inlet between April and October 2018. Sample labels on the vertical axes correspond to sampling month and water column depth. Vertical axis labels are color coded according to in situ dissolved oxygen concentrations.

N₂O-cycling was explored by evaluating relationships between ASV subnetwork membership, intranetwork connectivity (K_{in}), and ASV importance in predicting rate processes and water column N₂O saturations (ΔN_2O).

WGCNA clustered microbial ASVs into three discrete subnetworks (SNETs 1–3) containing 135, 77, and 150 ASVs, respectively (Table 1). These results were largely congruent with those identified through proportionality analyses, with taxa separating broadly into three primary clusters according to their subnetwork assignments identified through WGCNA (Fig. 3). SNET1 was inversely correlated with dissolved O₂ ($r = -0.75$, $p = 3 \times 10^{-4}$), ΔN_2O ($r = -0.65$, $p = 0.004$), and $[NO_3^- + NO_2^-]$ ($r = -0.89$, $p = 9 \times 10^{-7}$), and positively correlated with N₂O production from NO₃⁻ reduction ($r = 0.61$, $p = 0.007$) as well as N₂O yields from nitrification ($r = 0.55$, $p = 0.02$) (Fig. 4, Table 1). A total of 81 SNET1 ASVs demonstrated significant positive correlations to rates of N₂O production from NO₃⁻ reduction ($r = 0.47$ – 0.75 , $p < 0.05$), while 52 ASVs correlated significantly with N₂O yields from nitrification ($r = 0.47$ – 0.65 , $p < 0.05$) (Supplementary Data 1). ASV membership to SNET1 was strongly correlated to ASV importance in predicting both N₂O production rates and nitrification yields, and inversely correlated with ΔN_2O (Fig. 4). Although SNET1 membership was also positively correlated with ASV importance in predicting rates of N₂O production from NH₄⁺ production, taxa-specific correlations were generally weak and insignificant (Fig. 4, Supplementary Data 1).

SNET2 and SNET3 represented nested subnetworks that displayed overlapping niche distributions and similar relationships

to environmental parameters and process rates (Fig. 4, Table 1). SNET2 was most strongly correlated to ΔN_2O ($r = 0.71$, $p = 0.001$) and $[NO_3^- + NO_2^-]$ ($r = 0.75$, $p = 3 \times 10^{-4}$), but was not significantly related to dissolved O₂ concentrations. In contrast, SNET3 demonstrated significant positive correlations to dissolved O₂ ($r = 0.83$, $P = 2 \times 10^{-5}$), $[NO_3^- + NO_2^-]$ ($r = 0.83$, $p = 2 \times 10^{-5}$), and ΔN_2O ($r = 0.52$, $p = 0.03$). Positive correlations observed between SNET2 and SNET3 and nitrification rates were not statistically significant at the subnetwork level ($r = 0.44$ and 0.38 , $p = 0.07$ and 0.10 , respectively) (Table 1). Regardless, we detected 25 bacterial ASVs with significant associations to nitrification rates ($r = 0.47$ – 0.65 , $p < 0.05$) and a strong positive correlation between ASV importance in predicting nitrification rates and ASV membership in SNET2 and SNET3 (Fig. 4, Supplementary Data 1). ASV membership in SNET2 and SNET3 was also strongly associated with water column ΔN_2O values, with a total of 42 ASVs demonstrating strong positive correlations ($r = 0.60$ – 0.89 , $p < 0.001$).

Keystone taxa linked to N₂O production processes. We extended our network inferences further by utilizing network topological indices of the proper covariance network to identify putative keystone taxa amongst core community members that correlated strongly with rate processes and water column N₂O saturations (ΔN_2O)⁵². We considered high node (ASV) degree, closeness centrality, and betweenness centrality measures as indicators of potential keystone status for microbial ASVs^{28,53,54}.

Core community taxa in SNET1 that correlated significantly with rates of N₂O production from NO₃⁻ reduction included highly connected members of the *Desulfobacteraceae*,

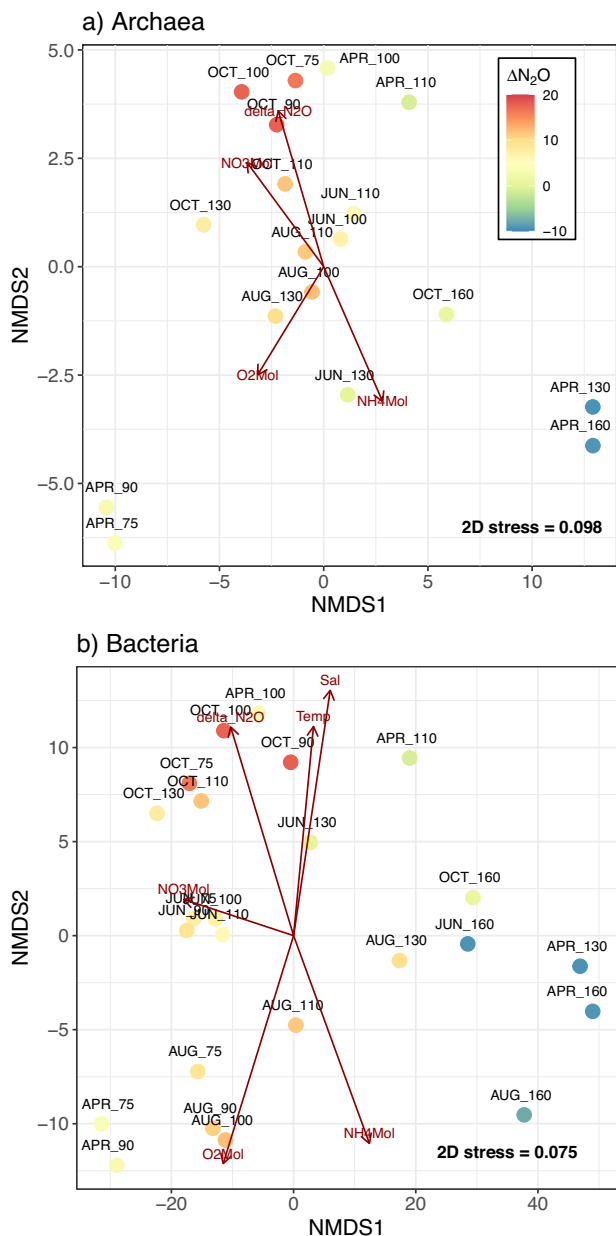


Fig. 2 Environmental drivers of community dissimilarity. Nonmetric multidimensional scaling (NMDS) ordinations for **a** Archaea and **b** Bacteria communities. NMDS analyses were conducted using Aitchison distances between samples calculated using clr-transformed ASV tables. Significant environmental predictors of community dissimilarity were calculated using *envfit* and the corresponding vectors are represented by red arrows.

Ectothiorhodospiraceae, Bacteroidales, and the SUP05 clade (Fig. 3, Supplementary Data 1). Other prominent ASVs related to N_2O production from NO_3^- reduction in SNET1 included members of the *Nitrosopumilus* and *Nitrospina* genera ($r = 0.51\text{--}0.59$, $p < 0.027$), as well as several unclassified members the α - and γ -proteobacteria, and Marinimicrobia. Core community members that correlated significantly with elevated nitrification rates and ΔN_2O belonged primarily to the SAR11 clade (11 of 25 ASVs) in addition to variants from the *flavobacteraceae* and MG II Euryarchaeota, which were generally well connected in SNET2 and SNET3 (Fig. 3, Supplementary Data 1). Additional taxa with high levels of connectivity in SNET2 and SNET3 that correlated strongly with ΔN_2O and demonstrated positive

associations with nitrification rates included four *Nitrosopelagicus*-like variants, and several *Rhodobacteraceae* and *Verrucomicrobiae* ASVs.

Microbial taxa that correlated well with N_2O production rates, nitrification rates, and ΔN_2O generally scored high on network topological indices of keystone status (Fig. 3b). However, several highly connected ASVs suggested by WGCNA as potentially important with respect to N_2O cycling were not classifiable below the class level and many were classifiable only at the kingdom level (Supplementary Data 1). Furthermore, results of the WGCNA demonstrating correlations between individual ASVs and rate processes are difficult to interpret given the large number of taxa implicated. In attempt to circumvent this issue, we fit a sparse partial least squares regression (sPLSR) model to predict sample traits from clr-transformed microbial ASV tables. sPLSR allowed us to elucidate robust taxa-specific links between individual ASVs and N_2O production processes by introducing a LASSO penalization to remove taxa with negligible effects⁵⁵. The final model was built using two latent components and a total of 60 microbial ASVs that separated broadly into four primary clusters (Fig. 5).

Cluster 1 contained eight bacterial and four archaeal ASVs, all of which belonged to SNET1 and correlated positively with N_2O production from NO_3^- reduction ($r = 0.38\text{--}0.60$) (Supplementary Data 2). The strongest taxon-specific correlations to rates of N_2O production from NO_3^- reduction ($r > 0.50$) were observed for ASVs that also correlated well with N_2O yields from nitrification ($r = 0.38\text{--}0.60$), which included *Nitrosopumilus* and SUP05 variants in addition to members of the Desulfobacterales, Marinimicrobia, Bathyarchaeia, and Thermosplasmata. In contrast, a subset of nine bacterial taxa within Cluster 4 demonstrated strong correlations to ΔN_2O ($r = 0.62\text{--}0.78$) and moderate correlations to nitrification rates >0.30 (Fig. 5). Taxa in this subcluster were also positively associated with dissolved O_2 and $NO_3^- + NO_2^-$ concentrations. ASVs included three SAR11 variants, three *Rhodobacteraceae* variants (including one *Amylibacter* ASV), one member of the *Puniceicoccaceae* (Verrucomicrobia MB11C04 Marine Group), and unclassified members of the α -proteobacteria and Marinimicrobia. Cross-referencing these results with those of our network analyses shows that individual ASVs implicated by sPLSR as strongest predictors of N_2O cycling rate were also implicated by our network analysis as potential keystone taxa with high closeness centrality and node degree (Fig. 3b, Supplementary Fig. 3).

Discussion

Spatiotemporal trends in microbial community structure were largely consistent with literature surveys of the Saanich Inlet water column over the seasonal stratification cycle^{46,56}. Vertical stratification of key microbial taxonomic groups was also in agreement with patterns of redox-driven niche partitioning observed in open ocean ODZs and other coastal anoxic basins^{10,11}. Given the extensive body of existing literature documenting patterns of microbial community composition across water column redox gradients and the well-characterized seasonal succession patterns observed in Saanich Inlet, we direct subsequent discussion toward key microbial players and community interaction networks implicated in N_2O cycling.

The Saanich Inlet archaeal community was dominated by thaumarchaeotal ASVs belonging to the *Nitrosopumilaceae* family, a highly supported monophyletic clade that contains all known members of the ammonium oxidizing archaea (AOA)⁵⁷. The majority of putative AOA sequences belonged to a single *Nitrosopumilus*-like ASV, which displayed broad water column distributions throughout the sampling period. This variant

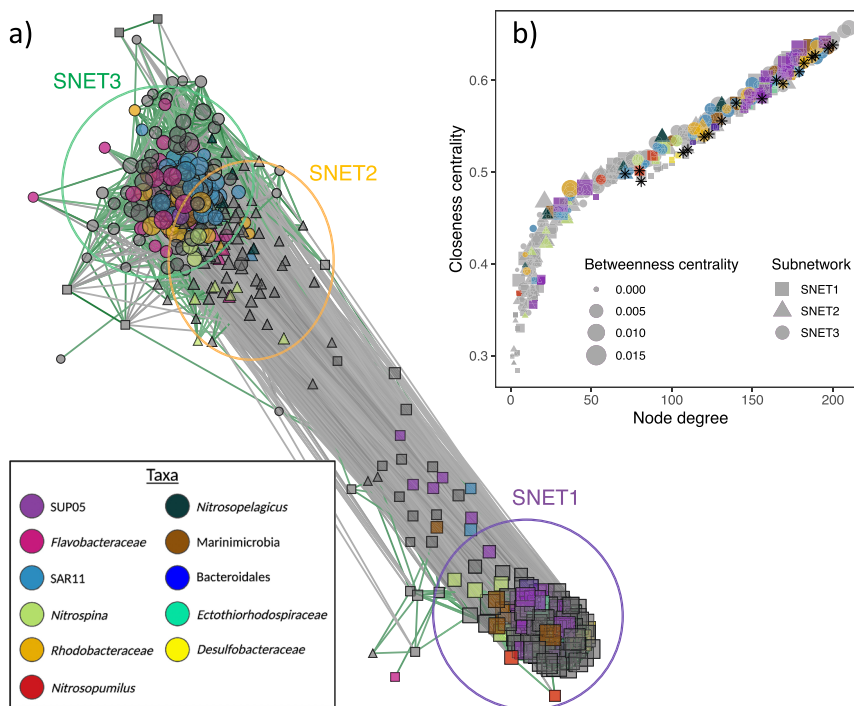


Fig. 3 Co-occurrence network depicting interactions between bacterial and archaeal ASVs in the Saanich Inlet microbiome. In panel **a** gray lines depict negative covariance and green lines depict positive covariance with $\rho > |0.60|$. Node size represents intranetwork connectivity (K_{in}) and shapes indicate subnetwork assignments determined by WGCNA. Squares, triangles, and circles represent taxa belonging to SNET1, SNET2, and SNET3, respectively, and are highlighted by colored circles. Taxonomic assignments are represented by colored nodes. Panel **b** depicts relationships between node (ASV) degree, closeness centrality, and betweenness centrality determined through analysis of the propr network. Individual ASVs implicated by sPLSR (Fig. 5) as important predictors of rate processes and ΔN_2O are indicated (*) in panel (**b**).

Table 1 Pairwise correlations between subnetwork (SNET) eigengenes and sample traits.

Environmental variables			Rate processes						
SNET	# of taxa	O ₂	ΔN_2O	NO ₃ ⁻ + NO ₂ ⁻	NH ₄ ⁺	Nitrification	NH ₄ ⁺ → N ₂ O	NO ₃ ⁻ → N ₂ O	N ₂ O yield
1	135	-0.75 (3e-04)	-0.65 (0.004)	-0.89 (9e-07)	0.72 (8e-04)	-0.42 (0.08)	0.21 (0.40)	0.61 (0.007)	0.55 (0.02)
2	77	0.36 (0.10)	0.71 (0.001)	0.74 (4e-04)	-0.73 (6e-04)	0.44 (0.07)	-0.078 (0.80)	-0.32 (0.20)	-0.49 (0.04)
3	150	0.83 (2e-05)	0.52 (0.03)	0.83 (2e-05)	-0.63 (0.005)	0.38 (0.10)	-0.25 (0.30)	-0.64 (0.004)	-0.49 (0.04)

Relationships are reported as Pearson's correlation coefficients with corresponding *p*-values (in parentheses). N₂O production rates from NH₄⁺ oxidation and NO₃⁻ reduction are symbolized by black arrows. Statistically significant correlations (*p* < 0.05) are bolded.

clustered together in SNET1 alongside two additional *Nitrosopumilus*-like ecotypes that were enriched in samples from the lower oxycline and anoxic basin. Members of the *Nitrosopumilus*-like ecotype are widely distributed across marine ecosystems, suggesting a role as generalists possessing broad environmental tolerances^{58–60}. *Nitrosopumilus*-like variants have been reported to dominate AOA communities in oxygen-depleted waters of other sulfidic basins, including the Baltic and Black Seas, and in ODZ waters of the Eastern Tropical South Pacific^{9,61,62}. Recent work has demonstrated oxygen production by *Nitrosopumilus maritimus* cultures as a means of supporting ammonium oxidation under anoxic conditions, indicating the presence of unique cellular machinery for maintenance during periods of severe oxygen limitation⁶³. In contrast, putative AOA variants related to the *Nitrosopelagicus* genus, which belong to the previously delineated water column group A (WCA) clade^{64,65}, clustered together in SNET2 and were most prevalent at oxycline depths.

Previous surveys of oxygen-deficient water columns have also demonstrated a preference of WCA-type AOA for oxygenated, epipelagic waters, suggesting that low-oxygen adaptation may not be universally distributed across all AOA clades^{62,66,67}.

Inferences based on experimentally derived rate measurements used in this study and relationships between ΔN_2O and apparent oxygen utilization indicate that N₂O production in Saanich Inlet is dominated by ammonium oxidation across oxycline depths^{44,51}. Similar to previous work in Saanich Inlet, we did not detect any sequences related to known ammonium oxidizing bacteria, suggesting that ammonium oxidation is predominantly mediated by AOA⁷. However, associations between biological variables and rates of N₂O production from ammonium oxidation were generally weak despite a significant correlation between the low-oxygen subnetwork (SNET1) and nitrification N₂O yields. Consistent with previous work, a substantial drop-off in overall nitrification rates was observed at O₂ concentrations less

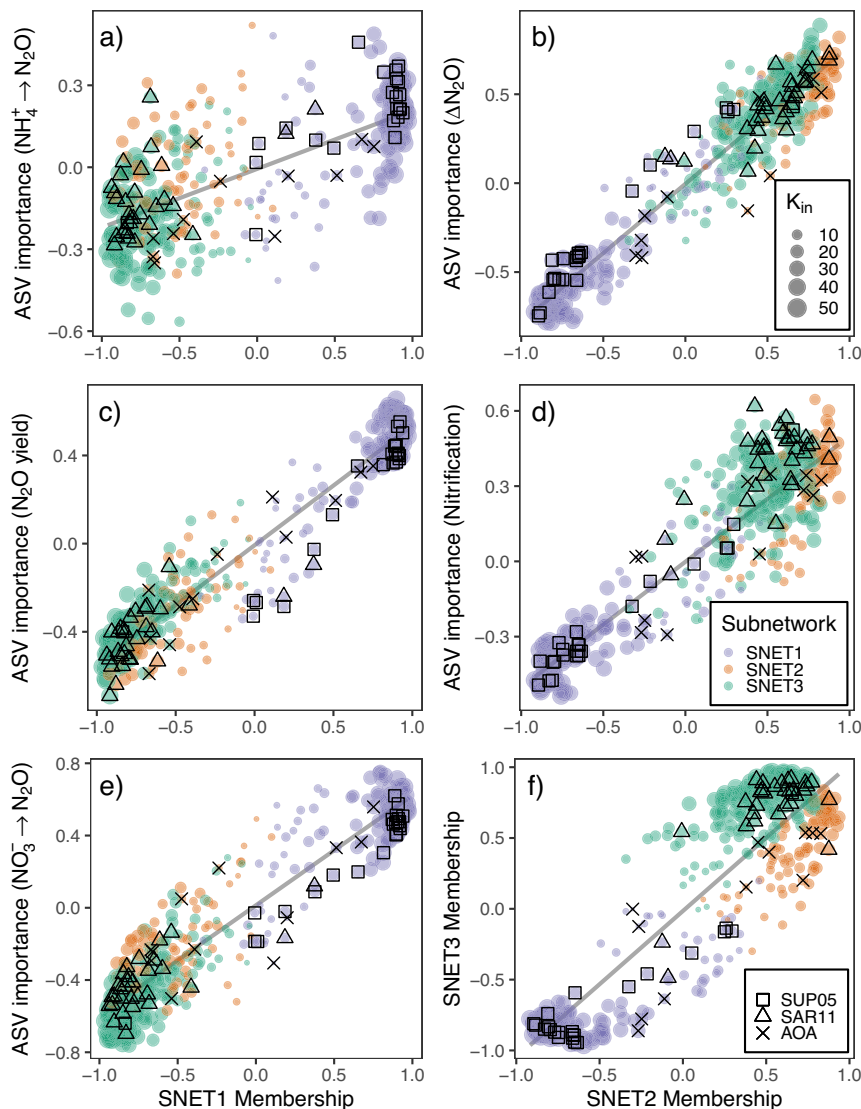


Fig. 4 Relationships between ASV subnetwork memberships and ASV importance in predicting various N_2O cycle proxies. Left panels depict relationships between SNET1 memberships and ASV importance in predicting **a** rates of N_2O production from NH_4^+ oxidation, **c** N_2O yields from nitrification, and **e** rates of N_2O production from NO_3^- reduction. Right panels depict relationships between SNET2 memberships and **b** $\Delta\text{N}_2\text{O}$, **d** nitrification rates, and **f** SNET3 memberships. ASV importance corresponds to the Pearson coefficients calculated for pairwise correlations between microbial ASVs and sample traits. Colors correspond to community subnetworks inferred from WGNA and bubble size indicates degree of intranetwork connectivity (K_{in}) for each ASV. Black squares, crosses, and triangles denote ASVs belonging to the SUP05 clade, the Nitrosopumilaceae family, and SAR11 clade, respectively.

than $1 \mu\text{mol L}^{-1}$ resulting in low overall N_2O production rates despite extremely high molar N_2O yields (Fig. 4a)^{51,68}. In contrast, maximum rates of N_2O production from NH_4^+ oxidation were measured at 160 m in October under suboxic conditions ($\text{O}_2 < 20 \mu\text{mol L}^{-1}$) following renewal of the deep basin⁵¹ (Fig. 4a). Injection of oxygen to the deep basin combined with high NH_4^+ concentrations in this case appears to have stimulated nitrification and the associated production of N_2O at relatively high yields.

Closer analysis of the data following removal of the October outlier point revealed a linear dependence of N_2O production rates from ammonium oxidation on overall nitrification rates (Fig. 4b). Furthermore, nitrification end products ($\text{NO}_3^- + \text{NO}_2^-$) and N_2O supersaturations were strongly associated with SNET2 and SNET3 communities (oxycline subnetworks hereafter), which contained distinct *Nitrosopelagicus*-like and *Nitrosopumilus*-like ecotypes. Water column N_2O

accumulation in Saanich Inlet thus appears driven primarily by *Nitrosopumilus*- and *Nitrosopelagicus*-like AOA variants at low to moderate yields across oxycline depths, with low- O_2 *Nitrosopumilus*-like ecotypes dominating the high-yield production of N_2O near the anoxic boundary and in the deep basin following oxygen renewal. However, putative nitrifying taxa (AOA or NOB) were not implicated by sPLSR or WGCNA as significant predictors of nitrification rates. We also did not detect any systematic variation in nitrification rates associated with dissolved O_2 or NH_4^+ concentrations (Supplementary Fig. 5), suggesting that alternative mechanisms may be responsible for regulating variability in nitrification rates, and thus N_2O accumulation across oxycline depths.

Consideration of community-wide dynamics showed that core community members belonging to oxycline subnetworks demonstrated stronger relationships to both nitrification rates and $\Delta\text{N}_2\text{O}$. Putative keystone taxa linked to nitrification rates

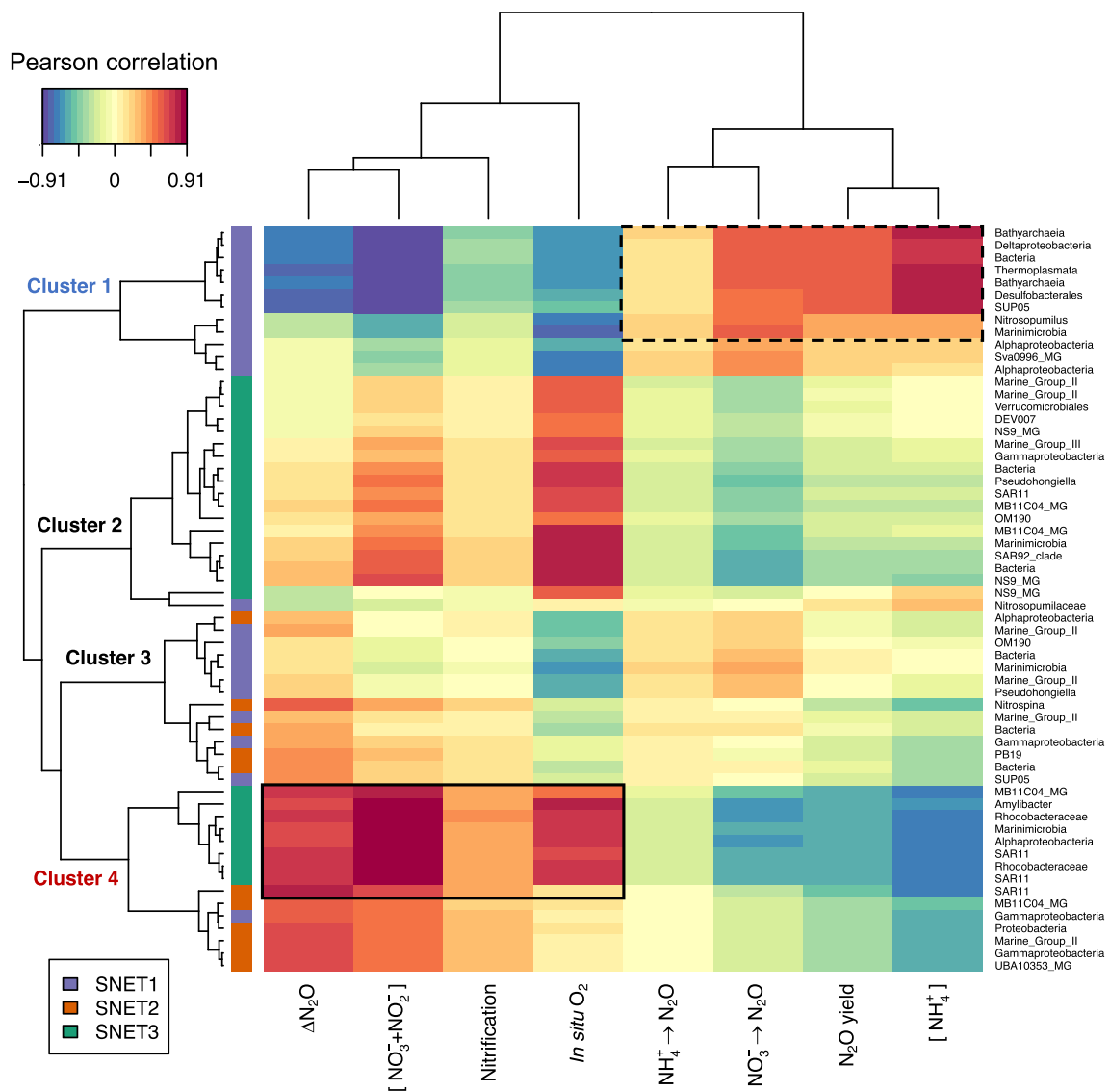


Fig. 5 Relationships between prokaryotic amplicon sequence variants (ASVs), relevant environmental variables, and process rates. N_2O production rates from NH_4^+ oxidation and NO_3^- reduction are symbolized by black arrows. Pairwise correlation coefficients between ASVs and sample traits were calculated using a two-component sPLS regression model and are presented as a clustered heatmap. Taxa with correlations to nitrification rates >0.30 are indicated by solid black lines and taxa with correlations to N_2O production from NO_3^- reduction >0.50 are indicated by dashed lines. Hierarchical clustering of variables was achieved using a complete Euclidean distance method. ASV subnetwork assignments determined through WGCNA are indicated by colored rectangles on the vertical axis dendrogram. Taxonomic labels correspond to the lowest level of classification determined for each ASV through alignment with the SILVA database.

belonged primarily to groups previously affiliated with the heterotrophic remineralization of organic matter, including the SAR11 α -proteobacteria, *Rhodobacteraceae*, *Flavobacteriaceae*, and MGII Euryarchaeota. These results were largely substantiated by the sPLSR analysis, which implicated prominent members of the SAR11 clade, *Rhodobacteraceae*, and *Puniceococcaceae* (Verrucomicrobia) as important predictors of $\Delta\text{N}_2\text{O}$ and nitrification rates. Members of the SAR11 clade are found ubiquitously throughout the global ocean and across ODZ redox boundaries, and generally possess streamlined genomes adapted for aerobic growth on dissolved organic carbon under oligotrophic conditions^{69,70}. Conversely, groups affiliated with the Verrucomicrobia, *Rhodobacteraceae*, *Flavobacteriaceae*, and MGII Euryarchaeota are commonly observed in association with phytoplankton blooms and may act as specialist consumers of various phytoplankton-derived carbon substrates^{71–74}. The

presence of proteorhodopsins in MGII metagenomes also suggests the potential for photoheterotrophic growth within the euphotic zone for this particular group⁷⁵.

Interestingly, taxa affiliated with many of these groups have been identified as keystone community members across a wide range of aquatic systems, further highlighting the importance of common aerobic heterotrophs in maintaining community stability and facilitating ecosystem function²⁸. For example, *Rhodobacteraceae* groups can form mutualistic cross-feeding relationships with pelagic diatoms whereby remineralized ammonium stimulates carbon fixation⁷⁶. Similarly, co-culture experiments using *Synechococcus* and *Roseobacter* populations have demonstrated that interactions between marine phototrophs and heterotrophs are stabilized over time through mutualistic nutrient cycling that involves leakage and subsequent remineralization of organic matter⁷⁷. Recent work has indicated that

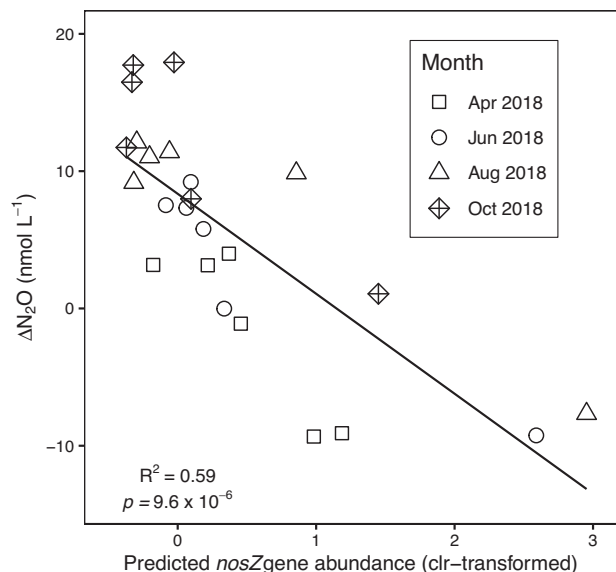


Fig. 6 Relationship between water column ΔN_2O (nmol L^{-1}) and PICRUSt2-predicted bacterial *nosZ* gene abundances. *NosZ* gene abundances were inferred from the predicted KEGG orthologues across all 24 samples using bacterial 16S rRNA amplicon sequences as input to the PICRUSt2 algorithm.

marine AOA also exude considerable amounts of labile dissolved organic matter, and that these exudates may support the growth requirements of auxotrophic heterotrophs such as SAR11⁷⁸. Indeed, regeneration of ammonium or urea from dissolved organic matter has been proposed as a potential mode of metabolic coupling between marine AOA and SAR11 based on metaproteomic surveys of the Saanich Inlet water column⁷. This is consistent with previous studies that have linked ammonium and nitrite oxidation rates to organic matter export and remineralization in marine water columns^{79,80}. These results collectively suggest that nitrification may be modulated through cross-feeding interactions with common aerobic heterotrophs occupying diverse niche spaces across oxycline depths.

Appreciable rates of N_2O production from NO_3^- reduction (hereafter denitrification), on the other hand, were primarily restricted to suboxic and anoxic depths, and were associated with putative keystone taxa belonging to the low-oxygen subnetwork. Prominent SUP05 ASVs were highly connected within the low-oxygen subnetwork and demonstrated robust taxa-specific correlations to N_2O production rates in both the WGCNA and sPLSR analyses. This is consistent with the role of SUP05 as core community taxa linking the biogeochemical cycling of nitrogen and sulfur in oxygen-depleted environments^{7,9,81}. Members of the SUP05 clade are abundant and active members of microbial communities across marine redox boundaries even in the absence of detectable levels of hydrogen sulfide and have been implicated as important drivers of autotrophic denitrification coupled to sulfide and elemental sulfur oxidation^{82–84}. Several mechanisms have been proposed to explain the persistence of SUP05 in sulfide-free waters, including intracellular storage of elemental sulfur or particle-associated micro-niches^{84–86}. Metagenomic and metaproteomic surveys of marine ODZs and coastal anoxic basins also indicate that the majority of SUP05 variants lack the metabolic machinery required to reduce N_2O to dinitrogen gas (N_2), leading to further speculation about a potential role in water column N_2O production^{7,81,87}. Given that SUP05 also appear as the only organisms in Saanich Inlet to express consecutive denitrification genes, our results provide further evidence that

SUP05 acts as an important mediator of N_2O production from denitrification⁷.

Several additional ASVs were also implicated by our analyses as potential keystone taxa with significant links to N_2O production from denitrification, including members of the Marinimicrobia, Bathyarchaea, *Ectothiorhodospiraceae*, Desulfobacterales, and Thermoplasmata. Whether these relationships reflect direct contributions to denitrification processes, ecological interactions with denitrifying taxa, or overlapping niche-preferences remains to be determined. Genes encoding components of the denitrification pathway are spread ubiquitously throughout the prokaryote domains with many taxa possessing only a partial complement of those required for complete denitrification, making it difficult to identify putative functional groups based on 16S rRNA sequences alone⁴. Furthermore, a considerable proportion of highly connected ASVs within the low-oxygen subnetwork were not classifiable below the phylum or class level, leaving much to be learned about the taxonomic affiliations and functional potentials of many potential core community members. Approximately half of the total denitrification proteins detected in Saanich Inlet belong to taxa other than SUP05⁷, indicating potential contributions to N_2O production facilitated by extracellular exchange of metabolic intermediates between modular components of the denitrification pathway. For example, we detected two low-oxygen SAR11 ecotypes, and recent analysis of single-cell genomes from the ETNP has uncovered novel ODZ variants that contribute to nitrogen loss processes via respiratory nitrate reduction⁷⁰.

As noted previously, elevated rates of N_2O production from denitrification were observed at depths depleted of nitrate and nitrite and were likely augmented by substrate enrichment following tracer additions⁵¹. However, putative nitrite-oxidizing bacteria (NOB) from the *Nitrospina* genus consisted of several low- O_2 ecotypes that were well-connected in the low-oxygen subnetwork alongside low-oxygen AOA ecotypes and correlated significantly with rates of N_2O production from denitrification. This correlation with denitrification supports previous reports of ecotype-specific metabolic interactions between AOA and NOB across depth-dependent environmental gradients and suggests the potential for N_2O production at lower oxycline depths driven by coupled nitrification-denitrification^{88–90}. Surveys of the Eastern Tropical North Pacific (ETNP) reported enrichment of novel *Nitrospina*-like variants at the upper ODZ boundary and within the ODZ core coinciding with relatively high rates of nitrite oxidation coupled to nitrate reduction^{91,92}. Measurable rates of nitrification were also detected at sub-micromolar oxygen concentrations during our sampling period⁵¹, and active ammonium and nitrite oxidation has been demonstrated in ODZ waters at oxygen concentrations as low as 5 nmol L^{-1} ^{51,68}. Regardless, taxa belonging to the low-oxygen subnetwork generally displayed strong negative correlations with water column ΔN_2O , and appreciable rates of N_2O production from denitrification were generally concomitant with pronounced N_2O undersaturation⁵¹. As a result, N_2O production near the anoxic interface appears offset by close coupling with N_2O consumption processes. Tight metabolic coupling between distributed elements of the denitrification pathway in Saanich Inlet may explain the low water column N_2O concentrations and surface N_2O fluxes relative to open ocean ODZs⁴⁴.

Several of the core community members identified in the low-oxygen subnetwork belong to taxonomic groups containing ODZ representatives that possess atypical N_2O reductases, such as the *Ectothiorhodospiraceae*, *Arcobacteraceae*, and *Bacteroidales*^{12,93}. PICRUSt2 predictions of bacterial *nosZ* gene abundances based on 16S rRNA sequences were negatively correlated with ΔN_2O (Fig. 6), supporting previous reports of elevated *nosZ* activity

within the Saanich Inlet deep basin⁷. Organisms possessing the atypical *nosZ* variant are commonly associated with higher N₂O affinities and lower O₂ sensitivities, and also typically lack additional genes in the denitrification pathway^{93–95}. A conceptual model describing mutualistic N₂O-cycling interactions has already been proposed in which N₂O produced by SUP05 is used by *nosZ*-harboring Marinimicrobia ecotypes to store polysulfide and regenerate H₂S¹². In contrast, atypical *nosZ* in the Bacteroidia class has been linked to particle-associated N₂O consumption while members of the *Arcobacter* genus in Saanich Inlet have been implicated in sulfide-driven denitrification^{93,96,97}. Atypical *nosZ* genes have also been identified in members of the *Ectothiorhodospiraceae*, a group generally associated with sulfide oxidation in anoxic environments^{93,98,99}. Given the inability of SUP05 in Saanich Inlet to reduce N₂O, these results indicate that N₂O consumption may be mediated through cross-feeding relationships involving diverse N₂O-reducing organisms that occupy varying ecological niches^{7,8}.

The results of our analyses provide statistical support for the presence of distributed metabolic networks mediating N₂O production and consumption in low-oxygen and sulfidic environments, and implicate additional groups involved in anaerobic sulfur cycling as potential keystone taxa. ASVs belonging to the *Desulfobacteraceae* family, for example, may supply sulfide to denitrifying organisms by coupling heterotrophic carbon oxidation to sulfate reduction^{83,100}. Metabolic coupling between chemolithotrophic denitrifiers and heterotrophic sulfate reducers may also help to explain the presence of detectable N₂O production rates from denitrification observed under well-oxygenated conditions following deep water renewal⁵¹. Appreciable rates of N₂O production from reductive processes were detected at oxycline depths with O₂ concentrations as high as 70 μmol L⁻¹ following summer and fall renewal events and were concomitant with high relative abundances of taxa from the low-oxygen subnetwork resulting from uplift of anoxic basin waters. Taxa from the low-oxygen subnetwork thus appear to serve as a net N₂O sink during periods of stable water column stratification yet maintain the capacity to respond rapidly to fresh inputs of terminal electron acceptors following renewal events, even under aerobic conditions. Re-supply of oxygen and fixed nitrogen species following deep-water renewal events therefore has the potential to simultaneously stimulate rates of N₂O production from all pathways and impede N₂O reduction within the deep basin, and may contribute to the elevated surface N₂O fluxes typically observed over fall months⁴⁴.

It is important to reiterate that specific findings obtained in a dynamic anoxic fjord that experiences both sulfide accumulation and transient oxygenation of the deep basin may not be extrapolatable to permanent open ocean ODZs. However, many of the interactions reported herein are centered around microbial constituents found ubiquitously throughout other sulfidic basins and open ocean ODZs, suggesting that similar relationships may be important determinants of microbial rate processes in other oxygen-deficient marine systems. Regardless, interpreting the underlying nature of specific co-occurrences revealed by network analyses is challenging, as interactions between taxa may reflect several ecological, environmental, or stochastic mechanisms. This is complicated further by the functional ambiguities associated with molecular marker profiling of natural microbial communities. Although improvements to the taxonomic resolution provided by shotgun metagenomics surveys may permit a more detailed assessment of microbial community interaction networks from a functional perspective, this would not eliminate the need to verify presumed ecological interactions empirically. A comprehensive view of how ecosystem function emerges from the cumulative influences of environmental variability and microbial

community dynamics will require careful experimentation guided by exploratory analyses to better understand the mechanisms that drive ecological interactions and co-evolution between microbial taxa over space and time.

Methods

Field sampling. Sampling was conducted bimonthly on the *MSV John Strickland* at a single location in Saanich Inlet (48° 37.53'N, 123° 29.91'W) on 5 April, 14 June, 02 August, and 25 October 2018 (Supplementary Fig. 1). The specifics of the sampling campaign, including chemical analyses and ¹⁵N-labeled tracer experiments to measure N₂O production rates from NH₄⁺ oxidation and NO₃⁻ reduction, have been detailed in Ji et al.⁵¹. Environmental proxies for N₂O production processes considered in the statistical analyses included dissolved O₂, N₂O saturation, as well as NO₃⁻ + NO₂⁻ and NH₄⁺ concentrations. N₂O saturation was defined as the N₂O excess, which is calculated from the concentrations difference between measured and expected equilibrium values with respect to the atmosphere. Seston samples for DNA sequencing were also obtained from the six discrete sampling depths (75, 90, 100, 110, 130, and 160 m) by filtering 5 L of seawater onto 0.2 μm Sterivex™ filters (Merck) by peristalsis. Samples designated for DNA extraction were immediately placed on dry ice, transferred to a -80 °C freezer later the same day, and stored for 6–12 months prior to extraction.

DNA extractions and high-throughput sequencing. Nucleic acids were extracted according to Crump et al.¹⁰¹ with the modifications suggested by Huber et al.¹⁰² and Sogin et al.¹⁰³. Sterivex filters were thawed, cut into strips, and placed in clean 2 mL microcentrifuge tubes containing 1 mL of DNA extraction buffer (1.5 M NaCl, 0.1 M Na-EDTA [pH 8.0], 0.1 M Tris-HCl [pH 8.0], 0.1 M NaH₂PO₄ [pH 8.0], and 5% cetyltrimethylammonium bromide; 0.2 μm filtered, autoclaved). Each tube was aliquoted with 20 μl of Proteinase K (10 mg/ml) and 40 μl of lysozyme (50 mg/ml) and then taken through three freeze-thaw cycles of 15 min at -80 °C and 5 min at 37 °C. Following the final freeze step, tubes were incubated at 37 °C for 30 min prior to addition of 50 μl sodium dodecyl sulfate (SDS; 20%; 0.2 μm filtered and autoclaved) and incubation in a water bath at 65 °C for 120 min. Tubes were then filled with phenol:chloroform:isoamyl alcohol (P:C:I; 25:24:1) to a final volume of ~2 ml, vortexed, and centrifuged (3000 rpm) for 5 min. The aqueous layer was transferred to a new 2 ml tube and the P:C:I addition, spin-down, and transfer steps were repeated a second time. DNA was precipitated by adding 0.6 volumes of molecular grade isopropanol (99.5%), mixing gently, and incubating at room temperature for 2 h. Samples were then centrifuged (13,000 rpm) for 30 min, washed with 1 ml of ethanol (70%), dried, and eluted in 150 μl of TE buffer (10 mM Tris-HCl [pH 8.0]; 1 mM Na-EDTA [pH 8.0]; 0.2 μl filtered, autoclaved). A sterile, blank Sterivex filter was included in each round of extractions, and the resulting material was carried through the PCR validation steps to ensure no contaminants were introduced during the extraction process. DNA extracts were cleaned using a QIAquick® PCR purification kit and DNA concentrations in cleaned extracts were quantified on a NanoDrop™ One Microvolume UV-Vis Spectrophotometer (Thermo Scientific).

The presence of target genes (16S rRNA) was verified by polymerase chain reaction (PCR) of genomic DNA (gDNA) using primers targeting the bacterial V6-V8 variable regions described by Comeau et al.¹⁰⁴ (Supplementary Table 1). PCR was conducted in 20 μl reaction volumes containing 4.0 μl 5X Green GoTaq™ reaction buffer (Promega), 2.0 μl dNTPs mixture diluted to final concentrations of 2.0 mM each (Thermo Scientific), 1.0 μl each of 2.0 μM forward and reverse primer (Eurofins Scientific), 10.8 μl UltraPure™ DNase/RNase-Free water (Invitrogen), 0.2 μl GoTaq™ DNA polymerase (Promega) and 1.0 μl template DNA. Thermal cycling began with an initial denaturation at 94 °C for 120 s, followed by 30 cycles of denaturation at 94 °C for 30 s, annealing at 55 °C for 45 s, extension at 72 °C for 120 s, and terminated following a final extension at 72 °C for 600 s. Bacterial and archaeal 16S rRNA genes were selected for sequencing from raw extracts using the same universal primer sets on an Illumina MiSeq at the Integrated Microbiome Resource (Dalhousie University, Halifax, Canada) using 2 × 300 bp paired-end V3 chemistry (<https://imr.bio/protocols.html>)¹⁰⁴. Final amplicon read lengths were 437 and 445 bp for Bacteria and Archaea, respectively. Bacterial 16S rRNA gene sequences were obtained from all samples, while archaeal sequences were obtained in 18 of 24 samples.

Demultiplexed reads were trimmed of primer-binding sequences using Cutadapt and reads with no primer match were discarded¹⁰⁵. Trimmed reads were then processed in USEARCH v1.1 to generate amplicon sequence variant (ASV) count tables¹⁰⁶. Bacterial and Archaeal 16S gDNA reads were merged using the *fastq_mergepairs* command with maximum allowable mismatches in the overlapping region (*fastq_maxdiffs*) set to 20 and the minimum percent ID of alignment (*fastq_pctid*) left on the default setting of 90. The trimmed and merged reads were then quality-filtered using a maximum expected error threshold (*fastq_maxee*) of 1.0 and ASV denoising was conducted on dereplicated sequences using UNOISE3¹⁰⁷. Singletons were removed and ASV tables were constructed with the *usearch_global* command using a similarity threshold of 99%. Since the denoising algorithm recovers the majority of true sequences in the sample, the 99% identity cut-off is fixed to allow for 1% error in the underlying reads believed to be

generated by sequencing and PCR errors. Taxonomies for 16S rDNA ASVs were inferred from the silva_nr_132 reference database in Mothur v1.42.3^{108,109}.

Statistics and reproducibility. Unless otherwise stated, statistical analyses and additional data-processing steps were conducted in the R Statistical Environment and followed best practices for the handling of compositional data^{110,111}. Imputation of zero-values was performed using Bayesian multiplicative replacement in the zCompositions package and read counts were converted to centred-log ratios (clr) prior to downstream analyses¹¹². Patterns of microbial community assembly were assessed using non-metric multidimensional scaling (NMDS) based on Aitchison distance matrices calculated across samples using the vegan package¹¹³. The *envfit* function was used to test for significant effects of environmental parameters on microbial community dissimilarity. We considered dissolved inorganic nitrogen concentrations (NH_4^+ , NO_3^- , NO_2^-), dissolved O_2 concentrations, water column N_2O saturations ($\Delta\text{N}_2\text{O}$), temperature, and salinity as potential predictors of microbial community structure.

Co-occurrence patterns between taxa with putative roles in N_2O production and the rest of the microbial community ASVs were explored using proportionality analysis within the propr package⁵². ASV tables were trimmed to select taxa that occurred ≥ 10 times in at least 10% of samples prior to network-level analyses to improve interpretability and minimize the risk of spurious correlations. Pairwise interactions between individual taxa with rho values greater than 0.60 were plotted using Cytoscape v3.9.0 and network topological indices were calculated using the NetworkAnalyzer tool¹¹⁴. Relationships between microbial community structure and rate processes were then assessed using weighted gene correlational network analysis (WGCNA) performed with the WGCNA package¹¹⁵. The signed adjacency measure was first calculated for each pair of features (ASVs) by raising the absolute value of their pairwise correlation coefficients to a soft-thresholding power of 8 to maximize the scale-free topology fit. Hierarchical clustering of taxa into discrete subnetworks was completed using a minimum module size threshold of 20 and a dissimilarity threshold of 0.3. Pearson correlation coefficients and corresponding *p*-values are reported for correlations between sample traits, subnetwork eigengenes, and individual ASVs (Supplementary Data 1). Subnetwork membership and intranetwork connectivity measures are also reported for each ASV and were used in further analyses to assess broad relationships between ASV connectivity and importance with respect to N_2O production rates.

Links between individual taxa and N_2O production processes inferred from WGCNA were then confirmed using sparse partial least squares regression (sPLSR), implemented in the MixOmics package¹¹⁶. The advantage of sPLSR is that it is capable of modeling highly dimensional datasets with multiple noisy and collinear variables, making it a useful method for exploring relationships between two continuous datasets when the total number of variables greatly outnumbers the number of discrete observations⁵⁵. This method combines dimension reduction and variable selection in a one-step modeling procedure, thus greatly improving interpretability over the standard PLSR approach. The final model was built after tuning based on Leave One Out cross-validation to determine the optimal number of latent components and variables for inclusion. Data sparsification is achieved by introducing a LASSO penalization to reduce the number of original variables used to construct the latent components. Pearson correlations between selected ASVs and sample traits were visualized in a clustered heatmap using a complete Euclidean distance method.

Detecting putative keystone taxa. We explored the potential role of keystone taxa in mediating N_2O production and accumulation by leveraging propr network topological indices to determine if taxa selected as important predictors of rate processes scored high on keystone measures. We considered high node (ASV) degree, closeness centrality, and betweenness centrality as indicators of microbial keystone taxa according to the recommendations of previous studies^{28,53,54,117}. Whereas node degree represents the number of edges (associations) a particular ASV shares with others in the network, closeness centrality measures the average distance of each node to other nodes in the network. In contrast, betweenness centrality calculates the extent to which a particular node lies on the shortest path between two adjacent nodes⁵⁴.

Community functional gene predictions. Bacterial community functional compositions were predicted using PICRUSt2 version 2.4.1 with the default settings to assess relationships between predicted *nosZ* gene abundances and water column N_2O saturations^{118,119}. Briefly, ASVs were placed within a reference phylogeny based on 20,000 16S sequences from the Integrated Microbial Genomes database by multiple sequence alignment using HMMER (<https://www.hmmmer.org>), optimal positioning of ASVs using EPA-ng¹²⁰, and phylogenetic tree reconstruction using GAPP¹²¹. The nearest-sequenced taxon index (NSTI) was calculated for each ASV and taxa with NSTI values less than 2.0 were excluded from downstream analyses. Less than 1% of bacterial ASVs (43 of 4674) were removed following quality filtering. Prediction of gene family abundances (including KEGG orthologues) was then conducted across samples using the Castor R package¹²². Predicted *nosZ* gene abundances were then selected from the model output based on the corresponding KEGG ortholog (K00376: nitrous-oxide reductase).

Reporting summary. Further information on research design is available in the Nature Portfolio Reporting Summary linked to this article.

Data availability

All chemical and rate measurement data used in this study have been published previously in the Pangaea Repository at <https://doi.org/10.1594/PANGAEA.912191>¹²³. Bacterial and archaeal 16S rRNA gene sequence data is accessible through the NCBI Sequence Read Archive (SRA) under BioProject number PRJNA901178. Results of network analyses and sPLSR used to construct Figs. 4 and 5 are contained in Supplementary Data 1 and Supplementary Data 2. Prokaryote ASV tables and predicted taxonomy files used to conduct statistical analyses and generate Figs. 1–3 can be accessed in the ‘Data’ folder at <https://github.com/bdjameson/Interaction-networks> under identifier <https://doi.org/10.5281/zenodo.7604057>¹²⁴. PICRUSt2 predictions generated using Bacterial ASV sequences are contained in the same GitHub repository under subfolder ‘PICRUSt2’.

Code availability

R code scripts used to process data and perform statistical analyses are available at <https://github.com/bdjameson/Interaction-networks> under identifier <https://doi.org/10.5281/zenodo.7604057>¹²⁴.

Received: 19 July 2022; Accepted: 15 February 2023;

Published online: 23 February 2023

References

- Fuhrman, J. A. Microbial community structure and its functional implications. *Nature* **459**, 193–199 (2009).
- Graham, E. B. et al. Microbes as engines of ecosystem function: when does community structure enhance predictions of ecosystem processes? *Front. Microbiol.* **7**, 214 (2016).
- Sunagawa, S. et al. Structure and function of the global ocean microbiome. *Science* **348**, 1261359 (2015).
- Graf, D. R. H., Jones, C. M. & Hallin, S. Intergenomic comparisons highlight modularity of the denitrification pathway and underpin the importance of community structure for N_2O emissions. *PLoS ONE* **9**, e114118 (2014).
- Louca, S., Parfrey, L. W. & Doebeli, M. Decoupling function and taxonomy in the global ocean microbiome. *Science* **353**, 1272–1277 (2016).
- Louca, S. et al. Function and functional redundancy in microbial systems. *Nat. Ecol. Evol.* **2**, 936–943 (2018).
- Hawley, A. K., Brewer, H. M., Norbeck, A. D., Paša-Tolić, L. & Hallam, S. J. Metaproteomics reveals differential modes of metabolic coupling among ubiquitous oxygen minimum zone microbes. *PNAS* **111**, 11395–11400 (2014).
- Louca, S. et al. Integrating biogeochemistry with multiomic sequence information in a model oxygen minimum zone. *Proc. Natl Acad. Sci. USA* **113**, E5925–E5933 (2016).
- Stewart, F. J., Ulloa, O. & DeLong, E. F. Microbial metatranscriptomics in a permanent marine oxygen minimum zone. *Environ. Microbiol.* **14**, 23–40 (2012).
- Ulloa, O., Canfield, D. E., DeLong, E. F., Letelier, R. M. & Stewart, F. J. Microbial ecology of anoxic oxygen minimum zones. *Proc. Natl Acad. Sci. USA* **109**, 15996–16003 (2012).
- Wright, J. J., Konwar, K. M. & Hallam, S. J. Microbial ecology of expanding oxygen minimum zones. *Nat. Rev. Microbiol.* **10**, 381–394 (2012).
- Hawley, A. K. et al. Diverse Marinimicrobia bacteria may mediate coupled biogeochemical cycles along eco-thermodynamic gradients. *Nat. Commun.* **8**, 1507 (2017).
- Falkowski, P. G., Fenchel, T. & DeLong, E. F. The microbial engines that drive Earth’s biogeochemical cycles. *Science* **320**, 1034–1039 (2008).
- Goldford, J. E. et al. Emergent simplicity in microbial community assembly. *Science* **361**, 469–474 (2018).
- MacLean, C. R., Dickson, A. & Bell, G. Resource competition and adaptive radiation in a microbial microcosm. *Ecol. Lett.* **8**, 38–46 (2005).
- Drescher, K., Nadell, C. D., Stone, H. A., Wingreen, N. S. & Bassler, B. L. Solutions to the public goods dilemma in bacterial biofilms. *Curr. Biol.* **24**, 50–55 (2014).
- Leão, P. N., Ramos, V., Vale, M., Machado, J. P. & Vasconcelos, V. M. Microbial community changes elicited by exposure to cyanobacterial allelochemicals. *Micro. Ecol.* **63**, 85–95 (2012).
- Cordero, O. X. & Polz, M. F. Explaining microbial genomic diversity in light of evolutionary ecology. *Nat. Rev. Microbiol.* **12**, 263–273 (2014).

19. Bálint, M. et al. Millions of reads, thousands of taxa: microbial community structure and associations analyzed via marker genes. *FEMS Microbiol. Rev.* **40**, 686–700 (2016).
20. Callahan, B. J. et al. DADA2: High-resolution sample inference from Illumina amplicon data. *Nat. Methods* **13**, 581–583 (2016).
21. Johnson, J. S. et al. Evaluation of 16S rRNA gene sequencing for species and strain-level microbiome analysis. *Nat. Commun.* **10**, 5029 (2019).
22. Barberán, A., Bates, S. T., Casamayor, E. O. & Fierer, N. Using network analysis to explore co-occurrence patterns in soil microbial communities. *ISME J.* **6**, 343–351 (2012).
23. Murdock, S. A., Tunnicliffe, V., Boschen-Rose, R. E. & Juniper, S. K. Emergent “core communities” of microbes, meiofauna and macrofauna at hydrothermal vents. *ISME COMMUN* **1**, 1–13 (2021).
24. Steele, J. A. et al. Marine bacterial, archaeal and protistan association networks reveal ecological linkages. *ISME J.* **5**, 1414–1425 (2011).
25. Guidi, L. et al. Plankton networks driving carbon export in the oligotrophic ocean. *Nature* **532**, 465–470 (2016).
26. Jones, C. M. et al. Recently identified microbial guild mediates soil N₂O sink capacity. *Nat. Clim. Change* **4**, 801–805 (2014).
27. Wang, S. et al. Investigating the microbial ecology of coastal hotspots of marine nitrogen fixation in the western North Atlantic. *Sci. Rep.* **11**, 5508 (2021).
28. Banerjee, S., Schlaeppi, K. & van der Heijden, M. G. A. Keystone taxa as drivers of microbiome structure and functioning. *Nat. Rev. Microbiol.* **16**, 567–576 (2018).
29. Li, F., Chen, L., Zhang, J., Yin, J. & Huang, S. Bacterial community structure after long-term organic and inorganic fertilization reveals important associations between soil nutrients and specific taxa involved in nutrient transformations. *Front. Microbiol.* **8**, 187 (2017).
30. Herren, C. M. & McMahon, K. D. Keystone taxa predict compositional change in microbial communities. *Environ. Microbiol.* **20**, 2207–2217 (2018).
31. Ravishankara, A. R., Daniel, J. S. & Portmann, R. W. Nitrous oxide (N₂O): the dominant ozone-depleting substance emitted in the 21st century. *Science* **326**, 123–125 (2009).
32. Arias, et al. in *Climate Change 2021: The Physical Science Basis. Contribution of Working Group I to the Sixth Assessment Report of the Intergovernmental Panel on Climate Change* (eds. Masson-Delmotte, V. et al.) 33–144 (Cambridge University Press, 2021).
33. Bange, H. W. et al. A harmonized nitrous oxide (N₂O) ocean observation network for the 21st century. *Front. Mar. Sci.* **6**, 157 (2019).
34. Bange, H. W., Freing, A., Kock, A. & Löscher, C. R. in *Nitrous Oxide and Climate Change* (ed. Smith, K. A.) 40–66 (Routledge, 2010).
35. Arévalo-Martínez, D. L., Kock, A., Löscher, C. R., Schmitz, R. A. & Bange, H. W. Massive nitrous oxide emissions from the tropical South Pacific Ocean. *Nat. Geosci.* **8**, 530–533 (2015).
36. Babbín, A. R., Bianchi, D., Jayakumar, A. & Ward, B. B. Rapid nitrous oxide cycling in the suboxic ocean. *Science* **348**, 1127–1129 (2015).
37. Ji, Q., Babbín, A. R., Jayakumar, A., Oleynik, S. & Ward, B. B. Nitrous oxide production by nitrification and denitrification in the Eastern Tropical South Pacific oxygen minimum zone. *Geophys. Res. Lett.* **42**, 10,755–10,764 (2015).
38. Bange, H. W. in *Nitrogen in the Marine Environment* (Second Edition) (eds. Capone, D. G., Bronk, D. A., Mulholland, M. R. & Carpenter, E. J.) 51–94 (Academic Press, 2008).
39. Devol, A. H. in *Nitrogen in the Marine Environment* (Second Edition) (eds. Capone, D. G., Bronk, D. A., Mulholland, M. R. & Carpenter, E. J.) 263–301 (Academic Press, 2008).
40. Anderson, J. J. & Devol, A. H. Deep water renewal in Saanich Inlet, an intermittently anoxic basin. *Estuar. Coast. Mar. Sci.* **1**, 1–10 (1973).
41. Gargett, A. E., Stocchi, D. & Whitney, F. Physical processes associated with high primary production in Saanich Inlet, British Columbia. *Estuar., Coast. Shelf Sci.* **56**, 1141–1156 (2003).
42. Grundle, D. S., Timothy, D. A. & Varela, D. E. Variations of phytoplankton productivity and biomass over an annual cycle in Saanich Inlet, a British Columbia fjord. *Cont. Shelf Res.* **29**, 2257–2269 (2009).
43. Anderson, J. J. & Devol, A. H. Deep water renewal in Saanich Inlet, an intermittently anoxic basin. *Estuar. Coast. Mar. Sci.* **1**, 1–10 (1973).
44. Capelle, D. W., Hawley, A. K., Hallam, S. J. & Tortell, P. D. A multi-year time-series of N₂O dynamics in a seasonally anoxic fjord: Saanich Inlet, British Columbia. *Limnol. Oceanogr.* **63**, 524–539 (2018).
45. Emerson, S., Cranston, R. E. & Liss, P. S. Redox species in a reducing fjord: equilibrium and kinetic considerations. *Deep Sea Res. Part A. Oceanogr. Res. Pap.* **26**, 859–878 (1979).
46. Michiels, C. C. et al. Rates and pathways of N₂ production in a persistently anoxic fjord: Saanich Inlet, British Columbia. *Front. Mar. Sci.* **6**, 27(2019).
47. Soetaert, G., Hamme, R. C. & Raftery, E. Renewal of seasonally anoxic Saanich Inlet is temporally and spatially dynamic. *Front. Mar. Sci.* **9**, 1001146 (2022).
48. Breitburg, D. et al. Declining oxygen in the global ocean and coastal waters. *Science* **359**, eaam7240 (2018).
49. Lavik, G. et al. Detoxification of sulphidic African shelf waters by blooming chemolithotrophs. *Nature* **457**, 581–584 (2009).
50. Schunck, H. et al. Giant hydrogen sulfide plume in the oxygen minimum zone off Peru supports chemolithoautotrophy. *PLoS ONE* **8**, e68661 (2013).
51. Ji, Q., Jameson, B. D., Juniper, S. K. & Grundle, D. S. Temporal and vertical oxygen gradients modulate nitrous oxide production in a seasonally anoxic fjord: Saanich Inlet, British Columbia. *J. Geophys. Res.: Biogeosci.* **125**, e2020JG005631 (2020).
52. Quinn, T. P., Richardson, M. F., Lovell, D. & Crowley, T. M. propr: an R-package for identifying proportionally abundant features using compositional data analysis. *Sci. Rep.* **7**, 16252 (2017).
53. van der Heijden, M. G. & Hartmann, M. Networking in the plant microbiome. *PLOS Biol.* **14**, e1002378 (2016).
54. Berry, D. & Widder, S. Deciphering microbial interactions and detecting keystone species with co-occurrence networks. *Front. Microbiol.* **5**, 219 (2014).
55. Cao, K.-A. L., Rossouw, D., Robert-Granié, C. & Besse, P. A sparse PLS for variable selection when integrating omics data. *Stat. Appl. Genet. Mol. Biol.* **7**, 35 (2008).
56. Zaikova, E. et al. Microbial community dynamics in a seasonally anoxic fjord: Saanich Inlet, British Columbia. *Environ. Microbiol.* **12**, 172–191 (2010).
57. Alves, R. J. E., Minh, B. Q., Ulrich, T., von Haeseler, A. & Schleper, C. Unifying the global phylogeny and environmental distribution of ammonia-oxidizing archaea based on amoA genes. *Nat. Commun.* **9**, 1517 (2018).
58. Hu, J. et al. Ecological success of the nitrosopumilus and nitrosospira clusters in the intertidal zone. *Micro. Ecol.* **78**, 555–564 (2019).
59. Müller, O. et al. Spatiotemporal dynamics of ammonia-oxidizing thaumarchaeota in distinct arctic water masses. *Front. Microbiol.* **9**, 24 (2018).
60. Reji, L., Tolar, B. B., Smith, J. M., Chavez, F. P. & Francis, C. A. Depth distributions of nitrite reductase (*nirK*) gene variants reveal spatial dynamics of thaumarchaeal ecotype populations in coastal Monterey Bay. *Environ. Microbiol.* **21**, 4032–4045 (2019).
61. Labrenz, M. et al. Relevance of a crenarchaeotal subcluster related to *Candidatus Nitrosopumilus maritimus* to ammonia oxidation in the suboxic zone of the central Baltic Sea. *ISME J.* **4**, 1496–1508 (2010).
62. Sollai, M., Villanueva, L., Hopmans, E. C., Keil, R. G. & Sinninghe Damsté, J. S. Archaeal sources of intact membrane lipid biomarkers in the oxygen deficient zone of the eastern tropical South Pacific. *Front. Microbiol.* **10**, 765 (2019).
63. Kraft, B. et al. Oxygen and nitrogen production by an ammonia-oxidizing archaeon. *Science* **375**, 97–100 (2022).
64. Santoro, A. E. et al. Genomic and proteomic characterization of “*Candidatus Nitrosopelagicus brevis*”: an ammonia-oxidizing archaeon from the open ocean. *Proc. Natl Acad. Sci. USA* **112**, 1173–1178 (2015).
65. Santoro, A. E. et al. Thaumarchaeal ecotype distributions across the equatorial Pacific Ocean and their potential roles in nitrification and sinking flux attenuation. *Limnol. Oceanogr.* **62**, 1984–2003 (2017).
66. Lu, Y., Xia, X., Cheung, S., Jing, H. & Liu, H. Differential distribution and determinants of ammonia oxidizing archaea sublineages in the oxygen minimum zone off Costa Rica. *Microorganisms* **7**, 453 (2019).
67. Muck, S. et al. Niche differentiation of aerobic and anaerobic ammonia oxidizers in a high latitude deep oxygen minimum zone. *Front. Microbiol.* **10**, 2141 (2019).
68. Bristow, L. A. et al. Ammonium and nitrite oxidation at nanomolar oxygen concentrations in oxygen minimum zone waters. *PNAS* **113**, 10601–10606 (2016).
69. Giovannoni, S. J. SAR11 bacteria: the most abundant plankton in the oceans. *Annu. Rev. Mar. Sci.* **9**, 231–255 (2017).
70. Tsementzi, D. et al. SAR11 bacteria linked to ocean anoxia and nitrogen loss. *Nature* **536**, 179–183 (2016).
71. Bakenhus, I. et al. Composition of total and cell-proliferating bacterioplankton community in early summer in the North Sea—roseobacters are the most active component. *Front. Microbiol.* **8**, 1771 (2017).
72. Teeling, H. et al. Recurring patterns in bacterioplankton dynamics during coastal spring algae blooms. *eLife* **5**, e11888 (2016).
73. Cardman, Z. et al. Verrucomicrobia are candidates for polysaccharide-degrading bacterioplankton in an arctic fjord of Svalbard. *Appl. Environ. Microbiol.* **80**, 3749–3756 (2014).
74. Orellana, L. H. et al. Verrucomicrobiota are specialist consumers of sulfated methyl pentoses during diatom blooms. *ISME J.* **16**, 630–641 (2022).
75. Pereira, O., Hochart, C., Auguet, J. C., Debros, D. & Galand, P. E. Genomic ecology of Marine Group II, the most common marine planktonic Archaea across the surface ocean. *MicrobiologyOpen* **8**, e00852 (2019).
76. Zecher, K., Hayes, K. R. & Philipp, B. Evidence of interdomain ammonium cross-feeding from methylamine- and glycine betaine-degrading *Rhodobacteraceae* to diatoms as a widespread interaction in the marine phycosphere. *Front. Microbiol.* **11**, 533894 (2020).

77. Christie-Oleza, J. A., Sousoni, D., Lloyd, M., Armengaud, J. & Scanlan, D. J. Nutrient recycling facilitates long-term stability of marine microbial phototroph–heterotroph interactions. *Nat. Microbiol.* **2**, 1–10 (2017).
78. Bayer, B. et al. Ammonia-oxidizing archaea release a suite of organic compounds potentially fueling prokaryotic heterotrophy in the ocean. *Environ. Microbiol.* **21**, 4062–4075 (2019).
79. Kalvelage, T. et al. Nitrogen cycling driven by organic matter export in the South Pacific oxygen minimum zone. *Nat. Geosci.* **6**, 228–234 (2013).
80. Santoro, A. E. et al. Nitrification and nitrous oxide production in the offshore waters of the Eastern Tropical South Pacific. *Glob. Biogeochem. Cycles* **35**, e2020GB006716 (2021).
81. Walsh, D. A. et al. Metagenome of a versatile chemolithoautotroph from expanding oceanic dead zones. *Science* **326**, 578–582 (2009).
82. Callbeck, C. M. et al. Oxygen minimum zone cryptic sulfur cycling sustained by offshore transport of key sulfur oxidizing bacteria. *Nat. Commun.* **9**, 1729 (2018).
83. Canfield, D. E. et al. A cryptic sulfur cycle in oxygen–minimum–zone waters off the Chilean coast. *Science* **330**, 1375–1378 (2010).
84. Callbeck, C. M. et al. Sulfur cycling in oceanic oxygen minimum zones. *Limnol. Oceanogr.* **66**, 2360–2392 (2021).
85. Shah, V. et al. Morphological plasticity in a sulfur-oxidizing marine bacterium from the SUP05 clade enhances dark carbon fixation. *mBio* **10**, e00216–e00219 (2019).
86. Bianchi, D., Weber, T. S., Kiko, R. & Deutsch, C. Global niche of marine anaerobic metabolisms expanded by particle microenvironments. *Nat. Geosci.* **11**, 263–268 (2018).
87. Murillo, A. A., Ramírez-Flandes, S., DeLong, E. F. & Ulloa, O. Enhanced metabolic versatility of planktonic sulfur-oxidizing γ -proteobacteria in an oxygen-deficient coastal ecosystem. *Front. Mar. Sci.* **1**, 1–18 (2014).
88. Reji, L., Tolar, B. B., Smith, J. M., Chavez, F. P. & Francis, C. A. Differential co-occurrence relationships shaping ecotype diversification within Thaumarchaeota populations in the coastal ocean water column. *ISME J.* **13**, 1144–1158 (2019).
89. Mincer, T. J. et al. Quantitative distribution of presumptive archaeal and bacterial nitrifiers in Monterey Bay and the North Pacific Subtropical Gyre. *Environ. Microbiol.* **9**, 1162–1175 (2007).
90. Parada, A. E. & Fuhrman, J. A. Marine archaeal dynamics and interactions with the microbial community over 5 years from surface to seafloor. *ISME J.* **11**, 2510–2525 (2017).
91. Peng, X. et al. Ammonia and nitrite oxidation in the Eastern Tropical North Pacific. *Glob. Biogeochem. Cycles* **29**, 2034–2049 (2015).
92. Sun, X., Frey, C., García-Robledo, E., Jayakumar, A. & Ward, B. B. Microbial niche differentiation explains nitrite oxidation in marine oxygen minimum zones. *ISME J.* **15**, 1317–1329 (2021).
93. Bertagnolli, A. D., Konstantinidis, K. T. & Stewart, F. J. Non-denitrifier nitrous oxide reductases dominate marine biomes. *Environ. Microbiol. Rep.* **12**, 681–692 (2020).
94. Sanford, R. A. et al. Unexpected nondenitrifier nitrous oxide reductase gene diversity and abundance in soils. *Proc. Natl Acad. Sci. USA* **109**, 19709–19714 (2012).
95. Yoon, S., Nissen, S., Park, D., Sanford, R. A. & Löffler, F. E. Nitrous oxide reduction kinetics distinguish bacteria harboring clade I *NosZ* from those harboring clade II *NosZ*. *Appl. Environ. Microbiol.* **82**, 3793–3800 (2016).
96. Callbeck, C. M. et al. *Arcobacter peruensis* sp. nov., a chemolithoheterotroph isolated from sulfide- and organic-rich coastal waters off Peru. *Appl. Environ. Microbiol.* **85**, e01344–19 (2019).
97. Fernández-Gómez, B. et al. Ecology of marine Bacteroidetes: a comparative genomics approach. *ISME J.* **7**, 1026–1037 (2013).
98. Bertagnolli, A. D. et al. Bacterial diversity in the bottom boundary layer of the inner continental shelf of Oregon, USA. *Aquat. Microb. Ecol.* **64**, 15–25 (2011).
99. Beman, J. M. & Carolan, M. T. Deoxygenation alters bacterial diversity and community composition in the ocean's largest oxygen minimum zone. *Nat. Commun.* **4**, 2705 (2013).
100. Rabus, R. et al. in *Advances in Microbial Physiology* (ed. Poole, R. K.) Vol. 66, 55–321 (Academic Press, 2015).
101. Crump, B. C., Armbrust, E. V. & Baross, J. A. Phylogenetic analysis of particle-attached and free-living bacterial communities in the Columbia River, its estuary, and the adjacent coastal ocean. *Appl. Environ. Microbiol.* **65**, 3192–3204 (1999).
102. Huber, J. A., Butterfield, D. A. & Baross, J. A. Temporal changes in archaeal diversity and chemistry in a mid-ocean ridge seafloor habitat. *Appl. Environ. Microbiol.* **68**, 1585–1594 (2002).
103. Sogin, M. L. et al. Microbial diversity in the deep sea and the underexplored 'rare biosphere'. *Proc. Natl Acad. Sci. USA* **103**, 12115–12120 (2006).
104. Comeau, A. M., Li, W. K. W., Tremblay, J.-É., Carmack, E. C. & Lovejoy, C. Arctic Ocean microbial community structure before and after the 2007 record sea ice minimum. *PLoS ONE* **6**, e27492 (2011).
105. Martin, M. Cutadapt removes adapter sequences from high-throughput sequencing reads. *EMBnet. J.* **17**, 10–12 (2011).
106. Edgar, R. C. Search and clustering orders of magnitude faster than BLAST. *Bioinformatics* **26**, 2460–2461 (2010).
107. Edgar, R. C. UNOISE2: improved error-correction for Illumina 16S and ITS amplicon sequencing. Preprint at *BioRxiv* <https://doi.org/10.1101/081257> (2016).
108. Quast, C. et al. The SILVA ribosomal RNA gene database project: improved data processing and web-based tools. *Nucleic Acids Res.* **41**, D590–D596 (2013).
109. Schloss, P. D. et al. Introducing mothur: open-source, platform-independent, community-supported software for describing and comparing microbial communities. *Appl. Environ. Microbiol.* **75**, 7537–7541 (2009).
110. Gloor, G. B., Macklaim, J. M., Pawlowsky-Glahn, V. & Egozcue, J. J. Microbiome datasets are compositional: and this is not optional. *Front. Microbiol.* **8**, 2224 (2017).
111. R. Core Team. R: A language and environment for statistical computing. R Foundation for Statistical Computing, Vienna, Austria. <https://www.R-project.org> (2021).
112. Palarea-Albaladejo, J. & Martín-Fernández, J. A. zCompositions—R package for multivariate imputation of left-censored data under a compositional approach. *Chemometr. Intell. Lab. Syst.* **143**, 85–96 (2015).
113. Oksanen et al. Community ecology package. R package version 2.6-2. <https://CRAN.R-project.org/package=vegan> (2022).
114. Shannon, P. et al. Cytoscape: a software environment for integrated models of biomolecular interaction networks. *Genome Res.* **13**, 2498–2504 (2003).
115. Langfelder, P. & Horvath, S. WGCNA: An R package for weighted correlation network analysis. *BMC Bioinform.* **9**, 559 (2008).
116. Rohart, F., Gautier, B., Singh, A. & Lê Cao, K.-A. mixOmics: an R package for 'omics feature selection and multiple data integration. *PLoS Comput. Biol.* **13**, e1005752 (2017).
117. Banerjee, S. et al. Network analysis reveals functional redundancy and keystone taxa amongst bacterial and fungal communities during organic matter decomposition in an arable soil. *Soil Biol. Biochem.* **97**, 188–198 (2016).
118. Douglas, G. M. et al. PICRUSt2 for prediction of metagenome functions. *Nat. Biotechnol.* **38**, 685–688 (2020).
119. Langille, M. G. I. et al. Predictive functional profiling of microbial communities using 16S rRNA marker gene sequences. *Nat. Biotechnol.* **31**, 814–821 (2013).
120. Barbera, P. et al. EPA-ng: massively parallel evolutionary placement of genetic sequences. *Syst. Biol.* **68**, 365–369 (2019).
121. Czech, L. & Stamatakis, A. Scalable methods for analyzing and visualizing phylogenetic placement of metagenomic samples. *PLoS ONE* **14**, e0217050 (2019).
122. Louca, S. & Doebeli, M. Efficient comparative phylogenetics on large trees. *Bioinformatics* **34**, 1053–1055 (2018).
123. Ji, Q. Temporal and vertical oxygen gradients modulate nitrous oxide production in a seasonally anoxic fjord: Saanich Inlet, British Columbia. *PANGAEA* <https://doi.org/10.1594/PANGAEA.912191> (2020).
124. Jameson, B. D. Community interaction networks. *Zenodo*. <https://doi.org/10.5281/zenodo.7604057> (2023).

Acknowledgements

This research was supported by the Canadian Healthy Oceans Network, the University of Victoria, the Bermuda Institute of Ocean Sciences, and an NSERC CGS-M award to B. Jameson. Field operations and laboratory analyses were partially supported by German Research Foundation (DFG) grants GR4721/2-1, MA6297/3-1) to D. Grundle and Christa Marandino (GEOMAR Helmholtz Centre for Ocean Research Kiel). We would like to thank Captain Ken Brown and the crew of the *MSV John Strickland* for their valued assistance with field operations. We would also like to thank Dr. Roberta Hamme, Erinn Raftery (UVic), and Amy Maas (BIOS) for their assistance with oxygen measurements. Finally, we would like to thank Alan Roberts for his guidance on the statistical analyses and Drs. Roberta Hamme and Caren Helbing for their valued comments on early manuscript drafts.

Author contributions

Details of the field sampling campaign and incubation experiments were conceived by Q.J., D.S.G., and S.K.J. Data acquisition was conducted by Q.J. and B.D.J. under the guidance of S.K.J., C.J.S., and D.S.G. Nucleic acids extractions, sequence processing and statistical analyses were performed by B.D.J. with the assistance of S.A.M. and C.J.S. The manuscript was written by B.D.J. with input from all authors.

Competing interests

The authors declare no competing interests.

Additional information

Supplementary information The online version contains supplementary material available at <https://doi.org/10.1038/s42003-023-04597-5>.

Correspondence and requests for materials should be addressed to Brett D. Jameson.

Peer review information *Communications Biology* thanks the anonymous reviewers for their contribution to the peer review of this work. Primary Handling Editor: George Inglis.

Reprints and permission information is available at <http://www.nature.com/reprints>

Publisher's note Springer Nature remains neutral with regard to jurisdictional claims in published maps and institutional affiliations.



Open Access This article is licensed under a Creative Commons Attribution 4.0 International License, which permits use, sharing, adaptation, distribution and reproduction in any medium or format, as long as you give appropriate credit to the original author(s) and the source, provide a link to the Creative Commons license, and indicate if changes were made. The images or other third party material in this article are included in the article's Creative Commons license, unless indicated otherwise in a credit line to the material. If material is not included in the article's Creative Commons license and your intended use is not permitted by statutory regulation or exceeds the permitted use, you will need to obtain permission directly from the copyright holder. To view a copy of this license, visit <http://creativecommons.org/licenses/by/4.0/>.

© The Author(s) 2023